Journal homepage: http://revues.imist.ma/?journal=jasi

ISSN: 2550-4800

https://doi.org/10.48442/IMIST.PRSM/jasi-v2i1-3.10562

Studies of dielectric relaxation and AC conductivity behavior in lamellar double hydroxide

A. Elmelouky [1,], A. Mortadi [1], E. Chahid [1], R. El Moznine [1], M.E. Belghiti [2].*

[1] *Laboratoire de Physique de La Matière Condensées (LPMC). Université Chouaib Doukkali, Faculté des sciences, El-Jadida, Morocco*
[2] *Laboratory of Applied Chemistry and Environment (URAC 18), Faculty of Sciences, University of Mohammed Premier, B.P. 4808, 60046 Oujda, Morocco*

Received 27 November 2017; Revised 18 J 2018; Accepted 21 February 2018.

Abstract: *Dielectric and electrical behaviors of this ionic clay were thoroughly investigated in the frequency range of 200 Hz to 1MHz. The clay was synthesized by co-precipitation method at room temperature. This sample was characterized by XRD, Fourier transform-infrared (FT-IR), inductively coupled plasma (ICP) and Thermogravimetric analysis. This sample was crystallized in a rhombohedral symmetry (Space group: R-3 m). Impedance spectroscopy was used as a tool to evaluate and monitor the activation process at different temperatures and frequency. The impedance measurement was well analyzed and fitted with an equivalent circuit containing (R//CPE). Furthermore, the AC conductivity σ_{ac} was also investigated as a function of frequency. It was analyzed and fitted using power law of Jonscher. These Studies show that the relaxation contribution is superimposed by electrode polarization effect.*

Keywords: *Materials physics; Materials Chemistry.*

1. Introduction

The industrial effluents originating in the activities of the textile sectors present an important coloring polluting load by its diversity, which each time requires to work out new means and new materials to remedy this pollution [1]. Recalcitrant organic, colored, and toxicant, surfactant and chlorinated compounds and salts are the main pollutants in textile effluents [2]. However, some azo dyes can show toxic effects, especially carcinogenic and mutagenic events [3]. The main environmental problems associated with the textile industry are typically those associated with water body pollution caused by the discharge of untreated effluents [4]. At the age of industrialization, environmental pollution is a matter of great concern. Surface water pollution is one of the elements of this pollution. Surface water is the water we find in the river, canals, cultivation field and other water bodies on the earth. Severe pollution of this water is causing serious health hazard in the neighborhood, damaging fertility of the land, killing fish and aquatic lives. Being a land of rivers Bangladesh is largely dependent on this surface water [5]. We must keep this water safe for better environment and good health of the people. Many issues are responsible for surface water pollution. Chemical processing industries, especially textile processing industries are claimed to produce huge effluent to discharge into our river and other water bodies [6]. Layered double hydroxides (LDH), also called anionic (anion-exchanging) clays and hydrotalcite-like compounds [7] are layered compounds that are based in brucite, $Mg(OH)_2$. They have a stacking of positively charged octahedral sheets with: $\left[M^{2+}_{1-x}M^{3+}_{x}(HO)_2\right]^{x+}$.

The compositions M^{2+} and M^{3+} are divalent and trivalent metal ions Zn and Al respectively. The net positive charge, due to substitution of trivalent by divalent metal ions, is balanced by an equal negative charge of Interlayer solvated anions: $\left[X^{m-}_{x/m}, xH_2O\right]^{x-}$, with X = Cl^-. Ion exchange is a technique commonly used to remove charged contaminants (anion and cation). The principle of this method is to circulate the contaminated water on a series of resins capable of exchanging these innocuous ions against the contaminants loaded with water. The use of this technique is somewhat limited because of the presence of other competitive anions such as sulfates; nitrate; fluor or phosphates [4].

The Lamellar Double Hydroxides (LDH) with a general formula: $[Zn_{1-x}Alx(OH)_2]x+[Xy.nH_2O]x-$, abbreviated as $[M^{2+}$-M^{3+}-X], with x= $(M^{2+}/(M^{3+}+M^{2+}))$[5]. The application of natural and abundant adsorbents such as synthesized clay for the treatment of water is a legitimate way to preserve water capital. The purpose of this work is to synthesize and characterize systems that have a very high adsorption capacity.

This research work has focused on the physicochemical characterization of Zn_2AlCl-LDH. Several techniques have been requested: DRX, ICP, FTIR, ATG and dielectric and electrical studies. It can be solicited to guide the use of these materials as needed.

* *Corresponding author: E-mail: elmlouky_abderrahmane@yahoo.fr (Abderrahmane Elmlouky)*

2. Experimental

2.1. Preparation

The Zn_2AlCl sample was synthesized by coprecipitation method with pH constant. Salts of $ZnCl_2$ ($AlCl_3$ $6H_2O$), such that the molar ratio (Zn^{2+}/Al^{3+} = 2) for the Zn_2AlCl sample. Once prepared and dissolved salts in decarbonated water, an addition of their solution to a solution of freshly prepared NaOH in decarbonated water should be done under nitrogen dropwise while maintaining the pH at 8. After pouring the entire solution of salts, the resulting colloidal mixture is stirred for 24 hours, well washed several times with decarbonated water, then dried 60 ° C for 48 h and ground into the fine for analysis.

2.1. Characterization Techniques

2.2.1. X-ray Diffraction

The X-ray diffraction patterns were carried out on D2-PHASER of BRUKER-AXS diffractometer which used $K\alpha_1$ (1.54056 Å) and $K\alpha_2$ (1.54439 Å). Generator used at 30 kV and 10 mA. Computation from 15 to 70° (2θ) by step of 0.0101° (0.2s by step). Program duration is 18mn 06 s.

2.2.2. Induced Coupled Plasma (ICP) Measurements

The metallic ratio what was performed using ICP measurements. A plasma or gas consisting of ions, electrons, and neutral particles, is formed from Argon gas, which is then utilized to atomize and ionize the elements in the sample matrix. These resulting ions are then passed through a series of apertures into a high vacuum mass analyzer, where the isotopes of the elements are identified by their mass-to-charge ratio. The intensity of a specific peak in the mass spectrum is proportional to the amount of the elemental isotope from the original sample, this technique of choice in many analytical for providing the accurate and precise measurements.

2.2.3. TGA-DTA Analysis

Thermogravimetric analyzes were carried out using a Mettler Toledo model Thermogravimetric Analyzer. The sample is heat-treated from 40°C to 450°C with a constant speed programmed at 20°C per minute. The nitrogen flow is 50 ml/min. The mass used of the sample is 30 mg.

2.2.4. Impedance Spectroscopy Measurement

The impedance measurements were carried out with a 4192 A LF Impedance Analyzer (Hewlett Packard) between 200 Hz and 1 MHz a source of 1V was applied to the electroded pellet sample. The temperature variation was performed using a hot stage with a temperature stability of ± 0.1 K. Silver electrodes were deposited on two circular faces of the sample to get the capacitor shaped sample. The diameter and the thickness of the sample were 13 mm and 1 mm, respectively. Curve fitting of dielectric spectra with complex empirical functions was carried out using commercial Zview software (Version 2.2).

3. Results and discussion

3.1. Structural Study

Fig. 1 shows the X-ray diffraction pattern of the sample Zn_2AlCl-LDH. From the analysis of the spectra, the material crystallizes in the R-3m space group (Rhombohedral phase) with: c/3 = d003 = 2×d006 and an (intermetallic distance) = 2×d110.

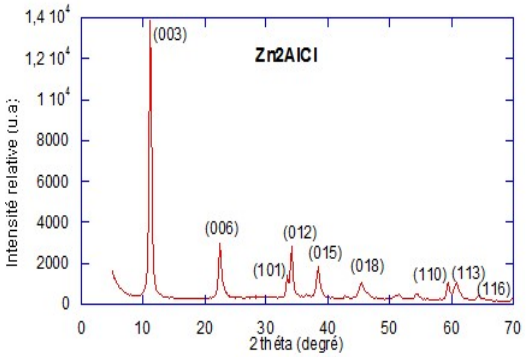

***Fig.1**. X-ray diffractogram of Zn_2AlCl*

Table 1

Values of the lattice parameters c, a and dinter for Zn_2AlCl.

sample	c(A°)	a(A°)	d_{inter}(A°)
Zn_2AlCl	23.717	3.1032	7.90

3.2. Induced coupled plasma (ICP)

The chemical compositions of the constituent LDH are included in Table 2, which shows that the [Zn^{2+}/Al^{3+}] ratio in the solids is close to that in the starting solutions. The formula in the table considers that chloride is the only compensating anion and does not take into account the possible presence of carbonate impurities in the interlayer space, even for Cl^-. The results of elemental analysis, which corresponds to the chemical formula:

($Zn_{1.95}$ Al (OH) 5.9)(Cl^-, 3.07 H_2O) for ratio R=2, X= Cl^-

Table 2

Elemental Chemical Analysis Data Metals ratio, (%) weight of H_2O, Al and Zn in Zn_2AlCl

(%) Zn	(%) Al	% (H_2O)	R_{exp}	R_{th}
36.9	7.8	15.94%	1.95	2

3.3. Infrared spectroscopy

Fig.2 shows the FT-IR spectra of Zn_2Al-Cl-LDH. Broad and intense bands at range of 3483–3493 cm^{-1} are ascribed to the O–H extending vibration in the brucite-like layers and the interlamellar water molecules [8]. The band at 1617 cm^{-1} designates the O–H bending vibration of the interlayer water molecules [9]. The augmentation of the band is qualified to hydrogen-bond formation [10].

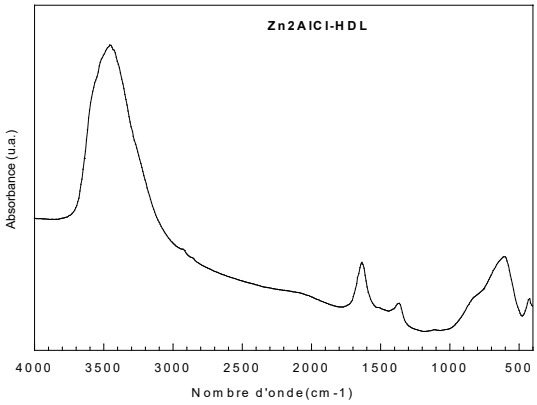

***Fig.2**. FT-IR spectra of Zn2AlCl-LDH*

Table 3

Absorbance bands of frequencies and powers of Zn_2AlCl-LDH

υ(OH)	υ(M-O)	δ(H_2O)	δ(O-M-O
3481.2 cm^{-1}	594.10 cm^{-1}	1628 cm^{-1}	426.28 cm^{-1}

3.4. Thermogravimetric Analysis (TGA)

Thermogravimetric analysis enables us to determine the different thermal events during heating. In general, the thermal evolution LDH phase involves three main events [11-13]. The Fig.3 complies with the behavior of an LDH. Indeed, between 295K and 475 K, a first mass loss of about 16% accompanied by an endothermic effect is observed. It corresponds to the removal of water adsorbed on the surface of the crystallites and interlamellar water. Because of dehydroxylation a sheet that also appears on the DTA curve endothermic phenomenon. Beyond 450°C begins the thermal decomposition of the intercalated anion (Cl^-) whose departure is in the form of HCl and also includes an endothermic effect [5] at the end of the thermal decomposition of LDH studied two compounds are obtained: Zinc oxide (ZnO) and the spinel phase $ZnAl_2O_4$ [14].

3.5. Analysis of impedance spectroscopy

The dielectric permittivity (ε’) in the LDH at different temperature can be seen in Fig.4. This Fig compares the variation of dielectric constant (ε’) with frequency for all temperatures. It has been observed that all of the samples exhibited relatively high dielectric permittivity at low frequencies and it increased with increasing the frequency [15]. The decrease of (ε’) with an increase in frequency may be attributed to the electrical relaxation processes, but at the same time, the material electrode polarization cannot be ignored, as the samples of our investigation are ionic conductors. The material electrode interface polarization superimposed with other relaxation processes at low frequencies. It is seen that with increases in temperature, value of permittivity increases [16].

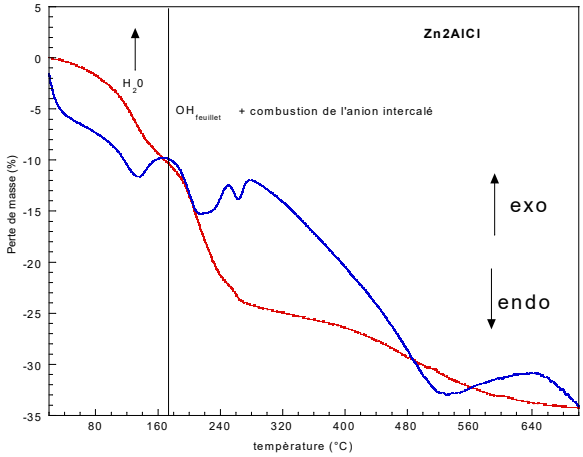

***Fig.3**. Thermogravimetric diagram of Zn2AlCl*

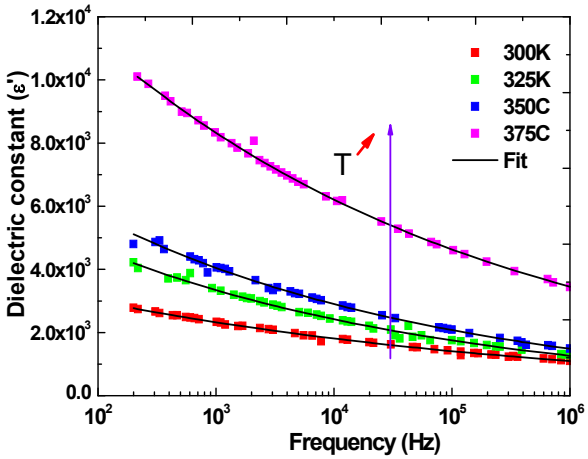

***Fig.4**. Variation of ε’ with frequency at all temperature.*

At low frequencies, the loss factor ε '' is greatly increased Fig.5. This is a consequence of the conductivity of the material. Indeed, the material is in the state or HDL ions have some degrees of freedom so that they can move and rearrange easily in the free volume '. In this case, the electric charges present in the material can move easily jump mainly through these channels and thus contribute to electrical conduction. This effect is particularly pronounced at the temperature 375K. Fig. 5 shows that ε″ decreased as the frequency increased, which can be attributed to an electrode polarization when the current carriers are dominant in the dielectric system [15].

The samples did not all have a slope of −1 for the imaginary dielectric constant. This result indicates the absence of Maxwell–Wagner polarization or DC conductivity in the frequency region studied [17]. The LDH contains a network of water molecules in the galleries between the layers that are hydrogen-bonded to the host lattice and to each other. The water molecules are also approximately the gallery ions (Cl^-) and may interact via complex formation or hydrogen bonding. The water molecule network of forms weakly connected clusters with partially ordered structure [18].

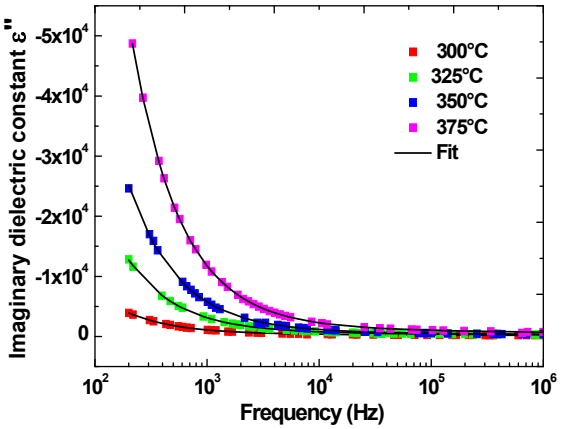

***Fig.5**. Variation of ε'' with frequency at different temperature.*

The conductivity σ*(ω) can be depicted as follows:

$$\sigma^*(\omega) = j\omega\varepsilon_0\varepsilon^*(\omega) \rightarrow \sigma'(\omega) = \omega\varepsilon_0\varepsilon''(\omega) \qquad (1)$$

where σ'(ω) is the real part of the conductivity, $\varepsilon_0 = 8.854*10^{-12}$ (F/m) is the absolute permittivity of free space, and ω=2πf, where f is the frequency. Fig.6 shows the variation of the real part of the conductivity (σ') with frequency at a different the temperature. The plateau region corresponding to dc conductivity is found to extend to higher frequencies when temperature increases. The frequency at which the dispersion takes place, also known as hopping frequency, increases with increasing of the temperature. This behavior suggests that electrical conductivity occurs via hopping mechanism, which is governed by the Jonscher universal power law [19]:

$$\sigma'(\omega) = \sigma_0 + A\omega^n \qquad (2)$$

(The solid line is the fit to the expression) where σ_0 is the dc conductivity (frequency independent plateau in the low frequency region), A is the pre-exponential factor and n is the fractional exponent between 0 and 1.

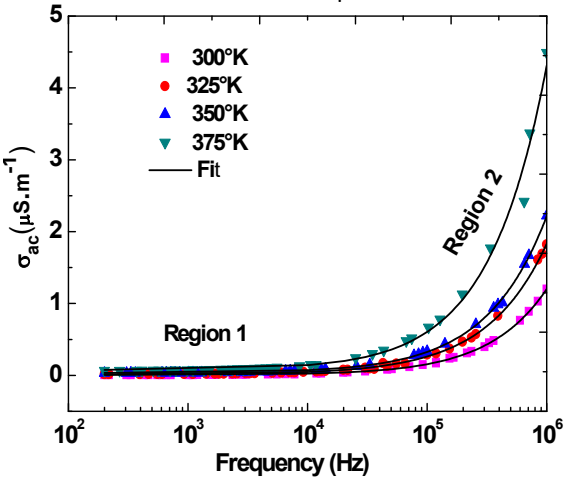

***Fig.6**. Variation of σ_{ac} with frequency for all temperature.*

The deviation from σ_{dc} (plateau region **1**) value in the conductivity spectrum is due to the electrode polarization effect. The values of σ_0, A, and n were obtained by fitting the Jonscher power law is tabulated in Table 4. Generally, for ionic conductors, power law exponents (n) can be between 1 and 0.5 indicating the ideal long-range pathways and diffusion limited hopping (tortuous pathway) respectively [20]. The value of the exponent of the higher frequency slopes (Table 4) shows that the long-range drift of ions may be one of the sources of ion conduction. From the Table 4, it is clear that the dc conductivity (σ_0) increases with increase in temperature.

Table 4

Parameters obtained from curve fitting by Jonscher low.

T (°C)	σ_{dc} (μS.m^{-1})	A	n	R^2
300	4.47E-03	4.96E-12	0.89	0.99
325	1.42E-02	1.18E-11	0.86	0.99
350	3.23E-02	1.30E-11	0.87	0.99
37	7.48E-02	1.63E-11	0.90	0.98

Another formalism based on the complex electrical module M*(ω) is generally proposed to minimize the effect of the conductivity [21]. This formalism has been used to study many materials [22,23] including glassy ionic conductors [24,25]. This formalism is currently adopted in the semi-crystalline polymers, composites, ceramics also LDH where existence over two different layers of permittivity and conductivity (at least two layers of composite materials). The complex modulus M * is defined as the inverse of the complex permittivity by the following equations:

$$M^* = (\varepsilon^*)^{-1} = M' + iM'' = \frac{\varepsilon'}{(\varepsilon')^2 + (\varepsilon'')^2} + j\frac{\varepsilon''}{(\varepsilon')^2 + (\varepsilon'')^2} \qquad (3)$$

Where M' and M'' represent the real part and the imaginary part of the electrical module respectively.

A comparison of the experimental data in the M* and ε* formalism is useful to distinguish long-range conduction process from the localized dielectric relaxation. To visualize this, we have plotted the imaginary part of the complex modulus (M'') as a function of frequency for all temperature Fig.7. Dielectric relaxation is a result of the reorientation process of dipoles in the LDH, which show a peak in M'' spectra. The vibration of ions Cl^- will perturb the electric potential of the surroundings. Motions of the other ions H in this region will be affected by perturbing potential. Such a cooperative motion of ions will lead to non-exponential decay, or a conduction processes with the distribution of relaxation time [26]. It has been observed that Fig.7 in the imaginary part of modulus spectra, a relaxation peak is observed for the conductivity processes at low frequency, whereas no peak is observed in the dielectric spectra Fig.5. This suggests that ionic motion is strongly coupled manifesting as a single peak in the M'' spectra with no corresponding feature in dielectric spectra [27].

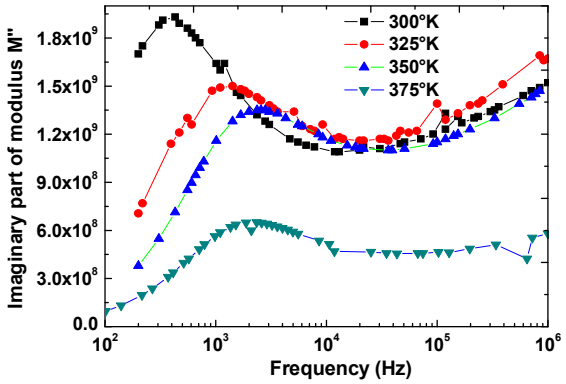

***Fig.7**. Variation of M'' with frequency for different temperature.*

The Fig.8 and Fig.9 (a, b) show the variations of the imaginary part and the real part of the complex permittivity as a function of frequency and temperature. At the same time, we find the separation of the low-frequency dispersion and the relaxation of Cole-Cole. The complex capacitance of LDH is influenced exponentially by variations in the reciprocal temperature and the relative humidity. The resulting complex capacitance shows low-frequency dispersion at high humidity and high temperatures, and a less dispersive power law at high frequencies, low humidity, and low temperatures.

The expression of permittivity is:

$$\varepsilon^*(\omega) = \varepsilon_\infty + \frac{\varepsilon_s - \varepsilon_\infty}{\left[1+\left(i\omega\tau_{mws}\right)^{\alpha}\right]} + \frac{\sigma_0}{i\omega\varepsilon_0} \qquad (4)$$

The complex permittivity can be written as:

$$\varepsilon^*(\omega) = \varepsilon'(\omega) - i\left[\varepsilon''(\omega) + \frac{\sigma_0}{\omega\varepsilon_0}\right] \qquad (5)$$

Therefore, this behavior could support that the low frequency dispersion LFD response could be describe very well by a power law in the analysis of our dielectric measurement.

$$\varepsilon_{LFD}{}^*(\omega) = \frac{\sigma_{ho}}{\varepsilon_0(i\omega)^{\beta}} \qquad (6)$$

In a more general approach the dielectric data could be described by using a superposition of two Cole–Cole relaxation functions and a power law taking into account the contribution the polarization of Maxwell–Wagner–Sillars (MWS).

$$\varepsilon^*(\omega) = \varepsilon_\infty + \frac{\Delta\varepsilon_{mws}}{\left[1+\left(i\omega\tau_{mws}\right)^{\alpha_{mws}}\right]} + \frac{\sigma_{ho}}{\varepsilon_0(i\omega)^{\beta}} \qquad (7)$$

The equation of the permittivity can be modeled by the equivalent circuit of permittivity (Fig.10). The equivalent circuit contains two blocks. A block that models LFD, the other models the relaxation of Cole-Cole.

In the Fig.8, low-frequency dispersion is very important in the representations of the real part of the permittivity. We also observe their importance on the representation of the imaginary part of the complex permittivity.

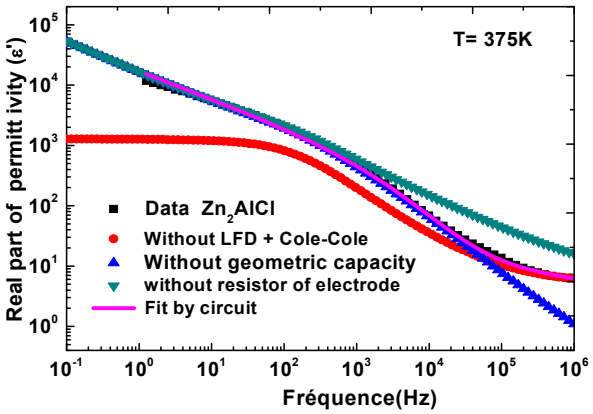

***Fig.8**. Variation of the real part of the complex permittivity.*

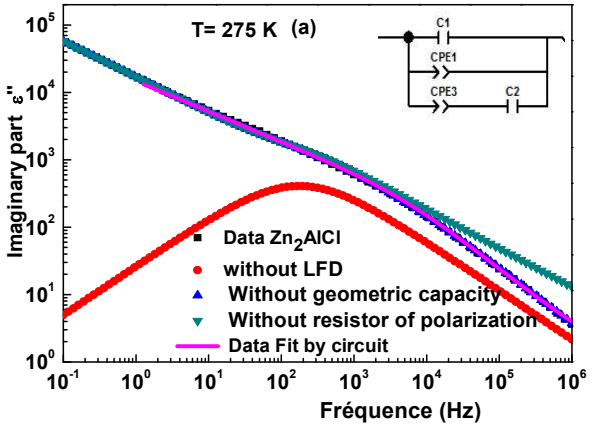

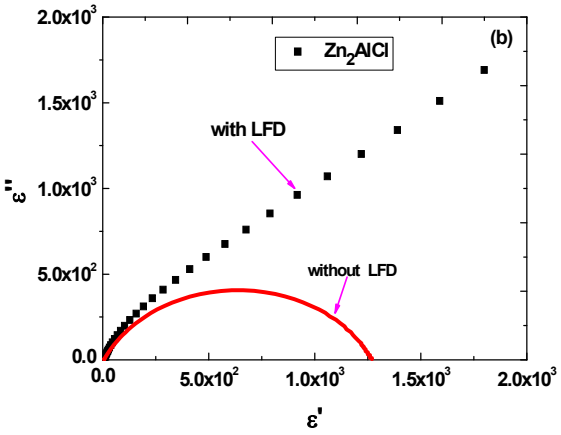

Fig.9(a,b) Variation of the imaginary part of the complex permittivity and LFD separation respectively.

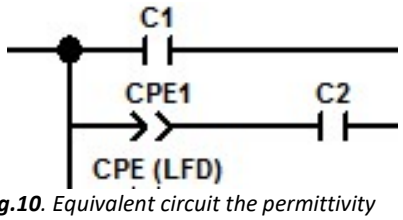

***Fig.10**. Equivalent circuit the permittivity*

4. Modeling the conductivity electrical using the circuit equivalent

The technique for interpret the results of dielectric spectroscopy is modeled by an electrical circuit equivalent, in this study we adopt this circuit that contains (R **//** CPE).

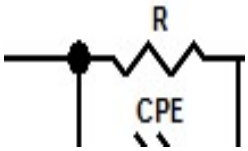

***Fig.11**. Equivalent electrical circuit*

The complex impedance (*Z**) of each element (CPE//R) is given by:

$$Z^*(\omega) = \frac{R}{1+(j\omega\tau)^p} \quad (4)$$

The relaxation time is given by the expression: $\tau^p = RT$ (5)

Finally, we find that by identifying expression,

$$Y^*(\omega) = \frac{1}{R} \times (1 + (j\omega\tau)^p)$$

the real part of conductivity was obtained from equation

$$\sigma'(\omega) = \frac{e}{S} Y'(\omega)$$

Finally, we found the expression of conductivity:

$$\sigma'(\omega) = \sigma_{dc} + A\,\omega^p \quad (6)$$

$$\sigma_{dc} = \frac{e}{s} \times \frac{1}{R} \quad , \quad A = \sigma_{dc} \times (\tau^p \cos\frac{p\pi}{2}) \quad (7)$$

Therefore, the Eq.(7) becomes the well-known Jonscher's power law given in Eq.(4). A good fit of the experimental data was obtained in the whole frequency range using the constant phase element (CPE) as shown in Fig.4. It is important to note that the modified equivalent RC circuit model with CPE. The resistances R_g, R_{bg}, and the parameters p and T of the CPE were obtained for each temperature. The values of p are found to lie close to unity (between 0.86 and 0.90). The constant time (τ) of relaxation were then obtained using the relationship given in Eq.(6).The increase in σ_{dc} conductivity with temperature is influenced by thermally activated drift mobility of ions. The activation energy for the thermally activated hopping process was obtained by fitting the σ_{dc} conductivity data with Arrhenius equation in Fig.12:

$$\sigma_{dc} = A \exp(\frac{-Ea}{KT}) \quad (8)$$

Where A is the pre-exponential factor, E_a is the activation energy for conduction and K is the gas constant.

The activation energy for Zn_2AlCl found by linear regression in the temperature range from 300K to 375K is 0.44 eV.

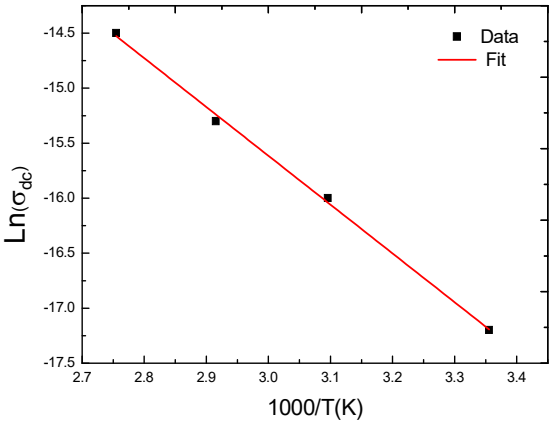

***Fig.12**. Variation of bulk conductivity Ln (σdc) as a function of (1000/T) (K-1) of Zn_2AlCl*

5. Conclusion

In this work, a good correlation between dielectric properties and the electrical conductivity was shown. Similar behavior has been seen in the evolution of electrical conductivity. However, electrical conductivity is only related to ionic transport properties for the free ions through the sample. Therefore, it will be very important to examine the alternative current conductivity (σ_{ac}) taken into account the characteristic relaxation times related to ionic translation individual or collective for a local movement of ions. For these reasons, other compositions are under investigation using impedance spectroscopy.

The frequency dependence of the ac conductivity follows the universal power law of Jonscher and the polarization of electrode is observed as the frequency limitation of our measurement tool.

The Conductivity spectra exhibited high conduction in high frequency region; the relaxation arises from the hopping conduction of created protons between the water molecules and from Cl^- ions in LDH interlayer. This clay is a good system for adsorbing toxic ions of small quantity

References

[1] C. Parvathi, T. Maruthavanan, C. Prakash, the Indian Textile Journal CXVII(2) (2009)22-26 .

[2] H.B. Mansour, I. Houas, F. Montassar, K. Ghedira, D. Barillier, R. Mosrati, L.C. Ghedira, Environmental science and pollution research international 19 (2012) 2634–2643.

[3] H.M. Pinheiro, E. Touraud, Thomas. Dyes and Pigments 61 (2) (2004) 121-139.
[4] K.T. Chung, C.E. Cerniglia. Mutation Research 277(3) (1992) 201-220.
[5] S. Miyata, Clays and Clay Minerals 23 (1975) 369-375.
[6] A.S.M Tareq Amin, M.E. Khan, 2009, Bangladesh Textile Today.
[7] D.A.B. Santos, F.J. Cervantes, V.J.B. Lier, Bioresource Technology 98(12) (2007) 2369-2385.
[8] A. Elmelouky, A. Mortadi, R. El Moznine, E. Chahid, R. Lahkale, E. Sabbar, International Journal of Advanced Research in Physical Science (IJARPS) 2(11) (2015) 1-10.
[9] M. Lakraimi, A. Legrouri, A. Barroug, A. De Roy, J P. Besse, Journal of Materials Chemistry 10 (2000) 1007- 1011.
[10] V.R. Allmann, Chimia 24 (1970) 99 -108
[11] S. Kim, E-J. Hwang, Y. Jung, Han M., Park S-J., Colloids and Surfaces A: Physicochemical and Engineering Aspects 313– 314 (2008) 216 -219.
[12] D.K. Pradhan, R.N.P. Choudhary, B.K. Samantaray, eXPRESS Polymer Letters 2 (2008) 630- 638.
[13] X. ZP, H.C. Zeng, Journal of Physical Chemistry B105 (2001) 1743- 1749.
[14] R.J. Carvajal, Journal of Materials Chemistry 7 (1997) 801-806.
[15] K.M. Parida, L. Mohapatr, Chemical Engineering Journal 179 (2012) 131-139.
[16] C. De la Calle, C-H. Pons, J. Roux, V. Rives, Clays and Clay Minerals 51 (2003)121-132.
[17] M. Oleinikova, M. Munoz, J. Benavente, M. Valiente, Analytica Chimica Acta 403 (2000) 91-99.
[18] A. Elmelouky, R. Elmoznine, R. Lahkale, R. Sadik, EL. Sabbar, E. Chahid, EL. Choukri, M. Daoud, Journal of Optoelectronics and Advanced Materials 15 (2013) 1239-1247.
[19] F. Carpi, D.D. Rossi, R. Kornbluh, R. Pelrin, P. Sommer-Larsen, Dielectric Elastomers as Electromechanical Transducers, Elsevier, Hungary (2008).
[20] N.A. Hegab, A.E. Bekheet, M.A. Afifi, L.A. Wahaba, H.A. Shehata, Journal of Ovonic Research 3 (2007) 71-82.
[21] C.R. Mariappan, G. Govindaraj, Materials Science and Engineering: B 94 (2002) 82-88.
[22] E.G. El-Metwally, M. Fadel, A.M. Shakra, M.A. Afifi, Journal of Optoelectronics and Advanced Materials 10 (2008) 1320-1327.
[23] A. Elmelouky, A. Mortadi, R. Elmoznine, E. Chahid, R. Lahkale, E. Sabbar, International Journal of Advanced Research 3(11) (2015) 465-475.
[24] K.A. Mauritz, Macromolecules 22(12) (1989) 4483–4488.
[25] N.G McCrum, B.E. Read, G. Williams, Anelastic and Dielectric Effects in Polymer Solids, Wiley, London, 1967.
[26] A. Arnoult, E. Dargent E., J.F. Mano, Polymer 48 (4) (2007) 1012-1019.
[27] P.B. Macedo, CT. Moynihan, R. Bose, Physics and Chemistry of Glasses 13 (1972) 171-179.
[28] F.S. Howell, R.A. Bose, P.B. Macedo, C.T. Moynihan, The Journal of Physical Chemistry 78 (1975) 639-648.
[29] Y. Fu, K. Pathmanathan, J.R. Steven, Journal of Chemical Physics 94 (1991) 6323-6330.
[30] P. Jeevanandam, J.Vasudevan, Journal of Chemical Physics 109 (1998) 8109-8117.